Improving volume-averaged particle-laden flow models using resolved simulations of particle diffusers

By M. Vartdal† AND S. S. Jain

Particle-resolved simulations of flows through random beds of fixed monodispersed particles with prescribed volume fraction gradients in the streamwise direction are used to create a database containing all terms in the volume-averaged flow equations. The simulations cover a range of inflow Mach and Reynolds numbers ($Ma \in [0.1, 0.2]$ and $Re \in [90, 300]$), as well as volume fraction gradients. The forces on the particles can be reasonably well predicted by a drag law developed for homogeneous flows. Furthermore, the pseudo-turbulent stress can be estimated using an algebraic closure if upstream volume fraction values are used. Finally, the average interface pressure, needed to close the volume-averaged equations, deviates from the commonly used phase-averaged pressure in a manner approximately scaling with the dynamic pressure, with systematic deviations correlating with the local volume fraction gradient.

1. Introduction

Compressible particle-laden flows play an important role in many applications of practical interest, such as liquid and solid fuel engines (Dittmann *et al.* 2011; Ren *et al.* 2019), explosive blast mitigation (Milne *et al.* 2010), and spacecraft landings on extraterrestrial bodies (Capecelatro 2022). For these systems, detailed experimental data is typically difficult to obtain and computational models are therefore a vital tool for investigation and design.

Recently there has been significant research effort aimed at improving volume-averaged particle-laden flow models. These efforts include improved estimation of forces on particles by accounting for pairwise interactions (Akiki *et al.* 2017*a*,*b*), improved estimates of sub-grid velocity variation (Osnes *et al.* 2019; Moore & Balachandar 2019), development of closure models for pseudo-turbulence (Mehrabadi *et al.* 2015; Vartdal & Osnes 2018; Shallcross *et al.* 2020), corrections appropriate when particle and mesh scales are of the same order (Horwitz & Mani 2016) and particle phase stress models (McGrath *et al.* 2016). These studies include both compressible and incompressible flow regimes and cover a large range of Mach and Reynolds numbers, as well as volume fractions. Despite these efforts, there are still a number of unanswered questions with regard to the closure of the volume-averaged equations. This is particularly true for high-speed two-way coupled configurations where model deficiencies easily lead to unphysical results (Theofanous & Chang 2017).

One way to investigate these issues is through particle-resolved simulations (Regele *et al.* 2014; Theofanous *et al.* 2018; Mehta *et al.* 2018; Osnes *et al.* 2020). Compared to experimental studies, these computations have the advantage of generating full-field data sets that are more useful for aiding modeling efforts. Most particle-resolved simulation

† Norwegian Defence Research Establishment, Norway

studies to date have been limited to either homogeneous configurations or particle curtains of constant volume fraction, and to the authors' knowledge, no systematic study on the effect of volume fraction gradients is available. In the present study, we aim to fill this gap by creating a database of particle-resolved simulation data for finite-Mach-number flows through random distributions of fixed particles with prescribed gradients in particle volume fractions. For all cases, the particle volume fraction is decreasing in the streamwise direction, and the particle bed effectively acts as a diffuser. The database contains all terms in the volume-averaged equations and covers a range of Mach numbers ($Ma \in [0.1, 0.2]$), Reynolds numbers ($Re \in [90, 300]$), and volume fraction gradients.

The resulting database can be used to explore questions concerning the closure problem of volume averaging for particle-laden flows. In the present work, we also investigate the validity of a particle drag and pseudo-turbulence closure model developed using assumptions of homogeneity. Furthermore, the dependence of the average interface pressure, used to close the volume-averaged equations (Crowe *et al.* 2011), on the flow conditions is also explored.

The remainder of the text is structured as follows: Section 2 contains the details of the problem set-up, Section 3 introduces the volume-averaged equations, Section 4 describes the computational method and discusses grid convergence, Section 5 contains the results of the analysis of the volume-averaged data, and Section 6 contains the concluding remarks.

2. Problem set-up

In the present study, particle-resolved simulations of flows through random beds of fixed monodispersed particles with prescribed volume fraction gradients in the streamwise direction are conducted. The geometry consists of an inflow region with an average gas-phase volume fraction $\alpha = 0.8$ of length $5D$, where D is the particle diameter, followed by a diffuser region of length L where the gas-phase volume fraction increases to 0.9. The diffuser region is followed by a constant volume fraction region of length $10D$ before the outflow boundary. A sketch of the set-up is found in Figure 1. The domain is periodic in the cross-stream directions with a width of $12D$. This results in approximately 55 and 27.5 particles per diameter in the streamwise direction for $\alpha = 0.8$ and 0.9, respectively. This domain width was chosen to give an acceptable balance between computational cost and accuracy in determining the volume fraction gradient. As seen in Figure 1, the realized volume fraction profile, generated by randomly drawing particles to fulfill the target distribution, introduces oscillations of the order of 5%.

Six different diffuser lengths ranging from $L/D = 1$ to $L/D = 30$ have been simulated. In addition, a geometry with a constant gas-phase volume fraction of 0.8 was also simulated. For this case, a total domain length of $30D$ was employed. The full list of diffuser lengths is found in Table 1, in which the constant volume fraction case is denoted by $L/D = \infty$.

The gas flow through the bed is governed by the compressible Navier-Stokes equations and the ideal gas equation of state with a constant specific heat capacity. Furthermore, a power law dependence of viscosity on temperature with an exponent of 0.75, along with a Prandtl number of 0.7, is used.

At the upstream boundary, a characteristic boundary condition with constant unit density, ρ, and temperature, T, along with a constant inflow velocity, u, is employed. The latter is set to obtain a superficial gas velocity $U = \alpha u = 1$. The viscosity of the fluid is

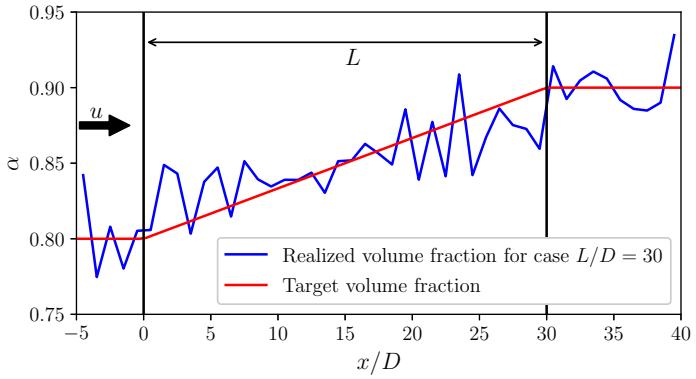

FIGURE 1. Case set-up for diffuser region of length $L/D = 30$. The blue curve is the realized gas-phase volume fraction computed using bins of width D, and the red line is the target volume fraction.

L/D \ Re_m, Ma_m	90			180			300		
	0.1	0.15	0.2	0.1	0.15	0.2	0.1	0.15	0.2
1	X	X	X	X	X	X	X	X	X
5	X	X	X	X	X	X	X	X	X
10	X	X		X	X	X	X	X	X
15	X	X		X	X		X	X	
20	X	X		X	X		X	X	
30	X	X		X	X		X	X	
∞	X			X	X		X	X	

TABLE 1. Overview of attempted simulations. An X indicates that a solution was obtained.

specified to realize the desired inflow Reynolds number $Re_m = \rho U D/\mu$, and the pressure is specified to obtain the target inflow Mach number $Ma_m = U/c$. At the particle surfaces, adiabatic wall boundary conditions are employed and at the downstream boundary, the mass flux is specified to match that of the inflow. For each geometry, simulations with three different Reynolds and Mach numbers were attempted. Table 1 gives an overview of the parameters for which successful simulation results were obtained.

3. Volume-averaged equations

The set-up described above is approximately one-dimensional in the volume-averaged sense. Let $\bar{\cdot}$ denote a volume-averaged quantity, $\langle\cdot\rangle$ a phase-averaged quantity, and $\tilde{\cdot} = \langle\rho\cdot\rangle/\langle\rho\rangle$ a Favre-averaged quantity. The corresponding Reynolds and Favre decompositions are given by $u = \langle u\rangle + u'$ and $u = \tilde{u} + u''$, respectively. The difference between the averages, $a = \tilde{u} - \langle u\rangle$, is commonly referred to as the turbulent mass flux (Schwarzkopf & Horwitz 2015). Using the above notation and the assumptions of steady flow, the governing volume-averaged equations simplify to

$$\frac{d}{dx}\left(\bar{\alpha}\langle\rho\rangle\tilde{u}\right) = 0, \tag{3.1}$$

$$\frac{d}{dx}\left(\alpha\langle\rho\rangle\tilde{u}\tilde{u}+\alpha\langle\rho\rangle\tilde{R}_{11}+\alpha\langle p\rangle-\alpha\langle\sigma\rangle_{11}\right)=\frac{1}{V}\int_S pn_1dS-\frac{1}{V}\int_S\sigma_{1k}n_kdS \tag{3.2}$$

and

$$\frac{d}{dx}\left(\alpha\langle\rho\rangle\tilde{E}\tilde{u}+\alpha\langle\rho\rangle\tilde{R}_{11}\tilde{u}+\alpha\langle p\rangle\tilde{u}-\alpha\langle\sigma_{11}\rangle\tilde{u}\right)=-\frac{d}{dx}\left(\alpha\langle\lambda\frac{\partial T}{\partial x}\rangle\right)-\frac{d}{dx}\left(\alpha\langle\rho e''u''\rangle\right)-$$
$$+\frac{d}{dx}\left(D^u+D^p+D^\mu+D^{ap}+D^{a\mu}\right). \tag{3.3}$$

Here, p is the pressure, σ is the viscous stress tensor, λ is the thermal conductivity, E is the total energy, e is the internal energy and $\tilde{R}_{11}=\widetilde{u''u''}$ is the streamwise component of the pseudo-turbulent stress. Furthermore, V denotes the averaging volume, S the continuous phase boundary in the averaging volume, $D^u=-1/2(\alpha\langle\rho u_i''u_i''u''\rangle)$ is the turbulent diffusion, $D^p=-\alpha\langle p'u'\rangle$ is the pressure diffusion, $D^\mu=\alpha\langle u_i'\sigma_{i1}'\rangle$ is the viscous diffusion, $D^{ap}=\alpha a\langle p\rangle$ is the pressure-diffusion effect due to the density-velocity correlation and $D^{a\mu}=-\alpha a\langle\sigma\rangle_{11}$ is the analogous viscous effect. In the above expressions, Einstein summation notation is used where necessary with $u=u_1$. Lastly, the integral terms on the right-hand side of Eq. (3.2) represent the momentum coupling between the two phases. It should be noted that for the highest Reynolds number, the flow becomes unsteady some distance downstream of the inlet. This introduces only minor oscillation in the volume averages and we approximate the flow as steady for the remainder of this paper.

The database of results contains all terms in the above equations for four different streamwise averaging lengths (D, $2D$, $4D$ and $5D$), as well as individual particle forces. The smaller averaging volumes are insufficient for the averages to be insensitive to averaging volume (see Figure 1). Nevertheless, analysis of the involved terms yields valuable insight into the governing equations.

The momentum coupling integrals of Eq. (3.2) deserve special attention. Following Crowe *et al.* (2011), the integral can be split into the contribution from the particles that are fully inside the volume-averaged region and the contribution from the particles that intersect the boundary. For the former, the integrals are equal to the sum of the forces on these particles and they can thus be closed with an appropriate force model. In the present stationary cases, this consists of the "buoyancy" contribution due to the pressure gradient and the steady drag contribution. With a slight abuse of notation, we express the sum of the particle forces per averaging volume as

$$\overline{F}_x=-(1-\alpha)\frac{d\langle p\rangle}{dx}-\frac{3}{4D}\alpha C_D\langle\rho\rangle\tilde{u}^2, \tag{3.4}$$

where C_D is an appropriate drag coefficient that must be supplied by a model.

For the particles that intersect the boundary, the integrals do not cover the entire surfaces of each particle and the mean contributions do not cancel. For simplicity, let us consider the pressure integral. If we introduce the decomposition $p=P_I+p'$, where P_I is the particle-surface-averaged (interface) pressure and p' is the deviation from that value, then, given that a sufficient number of particles intersect the control volume boundary, the contribution from the fluctuating part can be included with negligible bias in Eq. (3.4). On the other hand, P_I is unknown and requires a separate closure. In Crowe *et al.* (2011), P_I is approximated by $\langle p\rangle$, resulting in the phase-average pressure acting on the entire boundary of the volume-averaging region. This approximation is, however, not accurate for large relative velocities between the phases [see Chapter 3.3.1 of Osnes (2019) for

L/D	Re_m	Ma_m	Δ	$\max(\Delta\overline{F}_x/\lvert\overline{F}_x\rvert)$ 0.2D	0.1D	$\max(\Delta\tilde{R}_{11}/\tilde{R}_{11})$ 0.2D	0.1D	$\max(\Delta F_x/\lvert F_x\rvert)$ 0.2D	0.1D
5	90	0.1		0.057	0.003	0.036	0.008	0.059	0.008
5	180	0.1		0.079	0.012	0.0571	0.007	0.143	0.019
5	180	0.15		0.081	0.011	0.0501	0.009	0.143	0.015
5	180	0.2		0.072	0.013	0.0591	0.012	0.143	0.024
5	300	0.1		0.056	0.029	0.0702	0.019	0.271	0.189
20	90	0.1		0.024	0.003	0.0362	0.008	0.07	0.011
20	180	0.1		0.063	0.012	0.044	0.006	0.228	0.046
20	300	0.1		0.078	0.029	0.0514	0.04	0.291	0.246

TABLE 2. Grid convergence results. The volume-averaged data is based on bins of width $1D$.

details]. Therefore, the interface average values of pressure and viscous stress tensors are also included in the database.

4. Computational method

The particle-resolved simulations were performed using the compressible Navier-Stokes solver charLES from Cascade Technologies (Bres *et al.* 2018). It is a Voronoi-mesh-based code employing an entropy-stable numerical scheme (Masquelet *et al.* 2017). It has previously been used to study both shock-particle cloud interaction (Osnes *et al.* 2019, 2020) and drag forces on isolated spheres (Osnes & Vartdal 2022).

4.1. *Grid convergence*

The computational grids consist of a uniform background Voronoi-mesh with a resolution $\Delta = 0.1D$ and refinement zones in all volumes less than $0.1D$ from a particle surface. In the refinement regions, the grid length scale is set to $\Delta/4$, resulting in 40 grid points per diameter, which is similar to that used in Osnes *et al.* (2020).

A grid convergence test was carried out for a variety of Reynolds and Mach numbers for $L/D = 5$ and 20. Three different grid resolutions of $\Delta = 0.2D$, $0.1D$, and $0.05D$, with the same relative refinement level near the particle surface, were employed. The relative difference between the coarser grid results and the $\Delta = 0.05D$ results for volume-averaged particle forces, Reynolds stresses, and maximal individual particle force variation is reported in Table 2. As expected, the relative difference is primarily a function of the Reynolds number. For the two lowest Reynolds numbers, the maximal difference, for $\Delta = 0.1D$, for volume-averaged quantities is less than 1.5%, while for $Re_m = 300$ the difference is up to 4%. The latter is not insignificant and should be kept in mind when interpreting the results presented below.

For the individual particle forces, the same trend is observed. However, in this case the deviations are larger, with a maximal difference of 24.6% for $Re_m = 300$ and $L/D = 20$. Based on this, we conclude that a grid resolution of $\Delta = 0.1D$ is insufficient for evaluating individual particle forces at the highest Reynolds number. In the remainder of the paper, analysis is restricted to volume-averaged quantities.

5. Results

5.1. *Evaluation of drag law developed for homogeneous flow*

The momentum balance for the studied configurations is dominated by the pressure gradient and the forces acting on the particles. This implies that an accurate drag law is paramount for achieving accuracy with volume-averaged flow models in these cases. Prior to the summer program, a drag law based on particle-resolved simulations of homogeneous (triple periodic) flow configurations that covers the volume fraction, Reynolds, and Mach number ranges considered here was developed. It takes the form

$$\begin{aligned} C_{\mathrm{D}}\left(\alpha, Re_{\mathrm{p}}, Ma_{\mathrm{p}}\right) =& \frac{C_{\mathrm{D,Loth}}(Re_{\mathrm{p}}, Ma_{\mathrm{p}})}{\alpha^2} + b_1\left(\alpha\right) \exp\left[-(1-\alpha)(100Ma_{\mathrm{p}})^{1/3}\right] \\ &+ b_2\left(\alpha, Re_{\mathrm{p}}\right) \exp\left[-(1-\alpha)\left(200Ma_{\mathrm{p}}\right)\right] + b_3(\alpha, Ma_{\mathrm{p}}), \end{aligned} \tag{5.1}$$

where $Re_{\mathrm{p}} = \langle\rho\rangle\tilde{u}D/\mu$, $Ma_{\mathrm{p}} = \tilde{u}/c$, and $C_{\mathrm{D,Loth}}$ is the drag law for an isolated sphere from Loth *et al.* (2021). $b_1\left(\alpha_{\mathrm{p}}\right)$ and $b_2\left(\alpha_{\mathrm{p}}, Re_{\mathrm{p}}\right)$ are the volume fraction correction identified by Tenneti *et al.* (2011), and b_3 is an additional correction. Note that the above model uses the local Favre-averaged velocity as input and not the undisturbed flow. The above model is preliminary, and the full details will be published in a separate work.

Since Eq. (5.1) was developed based on homogeneous flow simulations, its accuracy in the presence of volume fraction gradients is tested here by comparing its predictions to the simulation results based on average drag coefficients computed from bins of width D. Figure 2(a) shows that the drag law works quite well, with most model predictions falling within 10% of the simulation results. There is a weak trend of under-prediction by the model, especially for low drag coefficient values. This corresponds to high Reynolds numbers, and some of the discrepancies may be attributed to insufficient grid resolution. However, for the drag coefficients from the homogeneous regions, displayed in Figure 2(b), we observe significantly less under-prediction. This indicates that the observed increase in drag with volume fraction gradient is likely to be real. However, finding a simple functional relationship for the deviation turned out to be challenging and is left as an interesting topic for future work.

5.2. *Pseudo-turbulence closure model*

Based on the particle-resolved simulations of shock-particle cloud interaction, Osnes *et al.* (2019) proposed an algebraic closure model for the streamwise pseudo-turbulent stress. This model is based on the idea of decomposing the volume-averaged flow field into two parts: one region that moves at the particle velocity, denoted α_{sep} for separation, and another region that moves at the "free" stream velocity. This idea was also explored in Fox *et al.* (2020). With this assumption, the model for the pseudo-turbulent stress can be expressed as

$$\tilde{R}_{11} = \tilde{u}^2 \frac{\alpha_{sep}}{\alpha - \alpha_{sep}}. \tag{5.2}$$

The above relation can be inverted to obtain an expression for α_{sep}

$$\alpha_{sep} = \frac{\alpha}{1 + \tilde{u}^2/\tilde{R}_{11}}, \tag{5.3}$$

which can be evaluated using particle-resolved data. The results of Osnes *et al.* (2020) showed that α_{sep} is almost constant for a given Reynolds number in a homogeneous cloud. However, at the edge of the particle clouds, where volume fraction gradients are non-negligible, large variations were observed. In the present work, we have evaluated the

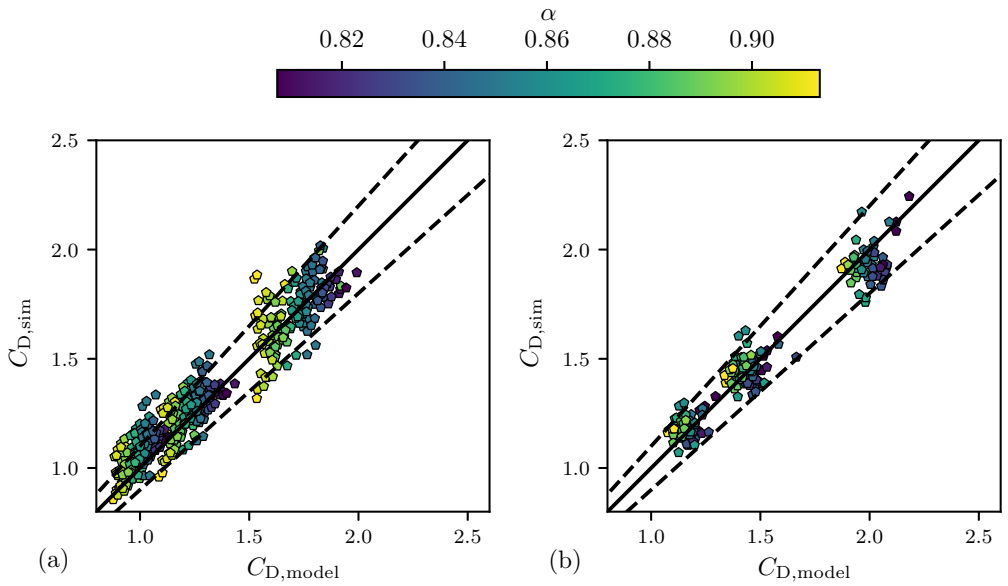

FIGURE 2. Particle-resolved bin-averaged drag coefficients versus the homogeneous-flow-based model in Eq. (5.1). (a) Diffuser regions. (b) Homogeneous regions. The symbols are colored by volume fraction. Dashed lines indicate a deviation of 10%. Only a representative subset of data is plotted for clarity.

average α_{sep} value for the regions with volume fraction gradients from all simulations. The results are shown in Figure 3(a). A clear trend of decreasing α_{sep} with L/D is observed, and the simple closure relation thus appears to be insufficient in the presence of volume fraction gradients. The idea behind the model, however, is to account for the separated flow volumes that appear behind the particles. Thus, it is reasonable to assume that the separation volume depends on the upstream volume fraction. Based on this observation, the average value of α_{sep} was recomputed using the volume fraction two diameters upstream of the averaging volume

$$\alpha_{sep}(x) = \frac{\alpha(x - 2D)}{1 + \tilde{u}^2(x)/\tilde{R}_{11}(x)}. \tag{5.4}$$

The results are displayed in Figure 3(b). With this adjustment, an almost constant separation volume is again observed. This is an encouraging result that suggests that algebraic closures for pseudo-turbulence may still be of use in the presence of gradients. Some variation is observed for the low-Reynolds-number and high-Mach-number cases, but this is likely due to the relatively large changes in flow conditions through the diffuser region.

5.3. *Average interface pressure*

From dimensional arguments, the difference between P_I and the phase-averaged pressure is likely to scale as the dynamic pressure. Therefore, the difference is plotted as a function of dynamic pressure in Figure 4. The data appears to scatter around a line of slope 1/4, and the deviation from this line is highly correlated with the gradient in volume fraction, as indicated by the color of the symbols. A positive gradient results in a smaller difference

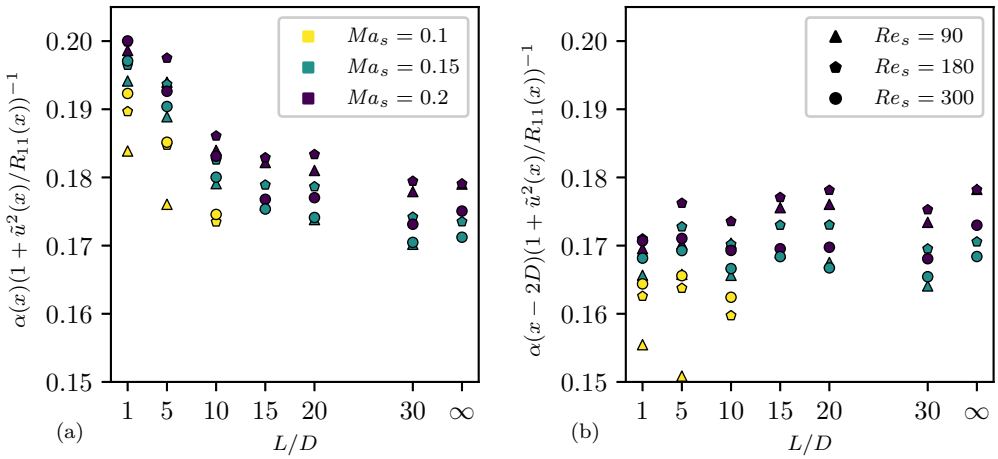

FIGURE 3. Equivalent separation region, α_{sep}, for pseudo-turbulence using (a) the original model from Osnes *et al.* (2019) and (b) an upstream value of the volume fraction. Symbols are colored by Ma_s.

and a negative gradient in a larger difference. From Eq. (3.1), we can deduce that the opposite correlation to flow acceleration is implied. The latter is somewhat intuitive, as one expects pressure differences to be correlated with accelerations.

In terms of relative values, pressure differences of the order of 10% of the phase-average were observed for some configurations. This implies that the adjusted closures for the volume-averaged equations are likely to have additional non-negligible terms scaling with $(1-\alpha)\langle\rho\rangle\tilde{u}^2$. Exploring the full mathematical implications of this observation is, however, deferred to future work.

6. Concluding remarks

In this study, particle-resolved simulations of flows through random beds of fixed monodispersed particles with prescribed volume fraction gradients in the streamwise direction have been used to create a database containing all terms in the volume-averaged flow equations. The simulation covered a range of Reynolds and Mach numbers as well as volume fraction gradients.

Analysis of the data revealed that a drag model developed based on simulations of homogeneous flow gives relatively accurate predictions. Volume fraction gradients appear to induce slightly higher values of drag, but more work is needed to establish accurate functional relationships. Furthermore, the applicability of the algebraic closure for pseudo-turbulence stresses presented in Osnes *et al.* (2019) was investigated. While the original model parameter displayed a dependence on the volume fraction gradient, the majority of this variation was eliminated by using an upstream value of the volume fraction, and the simplicity of the model can thus be preserved in the presence of gradients. Finally, the deviation of the average interface pressure, needed to close the volume-averaged equations, from the phase average was shown to approximately scale with the dynamic pressure, and deviations from this scaling were strongly correlated with the local volume fraction gradient. Formulation of a new closure of the volume-averaged equations based on these observations is deferred to future work.

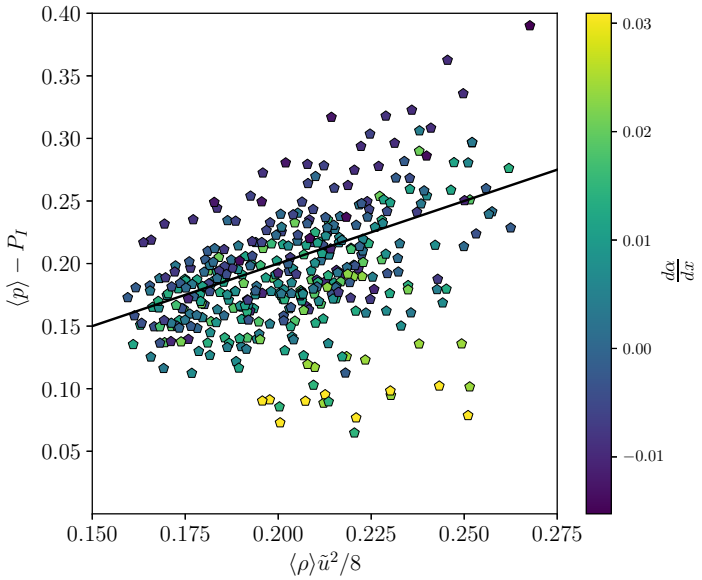

FIGURE 4. Pressure difference versus dynamic pressure computed from volume averages based on bins of width D. The symbols are colored by streamwise volume fraction gradient. The dark line represents a line of slope one.

Acknowledgments

The authors would like to thank A. N. Osnes, S. Balachandar, P. Johnson and S. T. Bose for many fruitful discussions. The authors acknowledge use of computational resources from the Yellowstone cluster awarded by the National Science Foundation to CTR.

REFERENCES

AKIKI, G., JACKSON, T. & BALACHANDAR, S. 2017*a* Pairwise interaction extended point-particle model for a random array of monodisperse spheres. *J. Fluid Mech.* **813**, 882–928.

AKIKI, G., MOORE, W. & BALACHANDAR, S. 2017*b* Pairwise-interaction extended point-particle model for particle-laden flows. *J. Comput. Phys.* **351**, 329–357.

BRES, G. A., BOSE, S. T., EMORY, M., HAM, F. E., SCHMIDT, O. T., RIGAS, G. & COLONIUS, T. 2018 Large-eddy simulations of co-annular turbulent jet using a Voronoi-based mesh generation framework. *AIAA Paper* 2018-3302.

CAPECELATRO, J. 2022 Modeling high-speed gas–particle flows relevant to spacecraft landings. *Int. J. Multiphas. Flow* **150**, 104008.

CROWE, C. T., SCHWARZKOPF, J. D., SOMMERFELD, M. & TSUJI, Y. 2011 *Multiphase Flows with Droplets and Particles*. CRC Press.

DITTMANN, T., JACOBS, G. & DON, W. S. 2011 Dispersion of a cloud of particles by a moving shock: effects of shape, angle of incidence and aspect ratio. *AIAA Paper* 2011-411.

FOX, R. O., LAURENT, F. & VIÉ, A. 2020 A hyperbolic two-fluid model for compressible flows with arbitrary material-density ratios. *J. Fluid Mech.* **903**, A5.

Horwitz, J. A. & Mani, A. 2016 Accurate calculation of Stokes drag for point–particle tracking in two-way coupled flows. *J. Comput. Phys.* **318**, 85–109.

Loth, E., Daspit, J. T., Jeong, M., Nagata, T. & Nonomura, T. 2021 Supersonic and hypersonic drag coefficients for a sphere. *AIAA J.* **59**, 3261–3274.

Masquelet, M., Yan, J., Dord, A., Laskowski, G., Shunn, L., Jofre, L. & Iaccarino, G. 2017 Uncertainty quantification in large eddy simulations of a rich-dome aviation gas turbine. In *ASME Turbo Expo 2017*, pp. 1–11. American Society of Mechanical Engineers.

McGrath, T. P., Clair, J. G. S. & Balachandar, S. 2016 A compressible two-phase model for dispersed particle flows with application from dense to dilute regimes. *J. Appl. Phys.* **119**, 174903.

Mehrabadi, M., Tenneti, S., Garg, R. & Subramaniam, S. 2015 Pseudo-turbulent gas-phase velocity fluctuations in homogeneous gas–solid flow: fixed particle assemblies and freely evolving suspensions. *J. Fluid Mech.* **770**, 210–246.

Mehta, Y., Neal, C., Salari, K., Jackson, T. L., Balachandar, S. & Thakur, S. 2018 Propagation of a strong shock over a random bed of spherical particles. *J. Fluid Mech.* **839**, 157–197.

Milne, A., Parrish, C. & Worland, I. 2010 Dynamic fragmentation of blast mitigants. *Shock Waves* **20**, 41–51.

Moore, W. & Balachandar, S. 2019 Lagrangian investigation of pseudo-turbulence in multiphase flow using superposable wakes. *Phys. Rev. Fluids* **4**, 114301.

Osnes, A. N. 2019 Shock-induced flow through particle clouds. PhD thesis, University of Oslo.

Osnes, A. N. & Vartdal, M. 2022 Mach and Reynolds number dependency of the unsteady shock-induced drag force on a sphere. *Phys. Fluids* **34**, 043303.

Osnes, A. N., Vartdal, M., Omang, M. G. & Reif, B. A. P. 2019 Computational analysis of shock-induced flow through stationary particle clouds. *Int. J. Multiphas. Flow* **114**, 268–286.

Osnes, A. N., Vartdal, M., Omang, M. G. & Reif, B. A. P. 2020 Particle-resolved simulations of shock-induced flow through particle clouds at different Reynolds numbers. *Phys. Rev. Fluids* **5**, 014305.

Regele, J. D., Rabinovitch, J., Colonius, T. & Blanquart, G. 2014 Unsteady effects in dense, high speed, particle laden flows. *Int. J. Multiphas. Flow* **61**, 1–13.

Ren, Z., Wang, B., Xiang, G., Zhao, D. & Zheng, L. 2019 Supersonic spray combustion subject to scramjets: progress and challenges. *Prog. Aerosp. Sci.* **105**, 40–59.

Schwarzkopf, J. D. & Horwitz, J. A. 2015 BHR equations re-derived with immiscible particle effects. *Tech. Rep*. Los Alamos National Laboratory.

Shallcross, G. S., Fox, R. O. & Capecelatro, J. 2020 A volume-filtered description of compressible particle-laden flows. *Int. J. Multiphas. Flow* **122**, 103138.

Tenneti, S., Garg, R. & Subramaniam, S. 2011 Drag law for monodisperse gas–solid systems using particle-resolved direct numerical simulation of flow past fixed assemblies of spheres. *Int. J. Multiphas. Flow* **37**, 1072–1092.

Theofanous, T. G. & Chang, C.-H. 2017 The dynamics of dense particle clouds subjected to shock waves. Part 2. Modeling/numerical issues and the way forward. *Int. J. Multiphas. Flow* **89**, 177–206.

Theofanous, T. G., Mitkin, V. & Chang, C.-H. 2018 Shock dispersal of dilute particle clouds. *J. Fluid Mech.* **841**, 732–745.

Vartdal, M. & Osnes, A. N. 2018 Using particle-resolved LES to improve Eulerian-Lagrangian modeling of shock wave particle cloud interaction. *Proceedings of the Summer Program*, Center for Turbulence Research, Stanford University, pp. 25–34.